Observation of Isolated High-E_T Photons in Photoproduction at HERA

ZEUS Collaboration

hep-ex/9708038   27 Aug 1997

Abstract

Events containing an isolated prompt photon with high transverse energy, together with a balancing jet, have been observed for the first time in photoproduction at HERA. The data were taken with the ZEUS detector, in a γp centre of mass energy range 120–250 GeV. The fraction of the incoming photon energy participating in the production of the prompt photon and the jet, x_γ, shows a strong peak near unity, consistent with LO QCD Monte Carlo predictions. In the transverse energy and pseudorapidity range $5 \leq E_T^\gamma < 10$ GeV, $-0.7 \leq \eta^\gamma < 0.8$, $E_T^{jet} \geq 5$ GeV, and $-1.5 \leq \eta^{jet} \leq 1.8$, with $x_\gamma^{\mathrm{OBS}} > 0.8$, the measured cross section is 15.3±3.8±1.8 pb, in good agreement with a recent NLO calculation.

The ZEUS Collaboration

J. Breitweg, M. Derrick, D. Krakauer, S. Magill, D. Mikunas, B. Musgrave, J. Repond, R. Stanek, R.L. Talaga, R. Yoshida, H. Zhang
Argonne National Laboratory, Argonne, IL, USA [p]

M.C.K. Mattingly
Andrews University, Berrien Springs, MI, USA

F. Anselmo, P. Antonioli, G. Bari, M. Basile, L. Bellagamba, D. Boscherini, A. Bruni, G. Bruni, G. Cara Romeo, G. Castellini[1], L. Cifarelli[2], F. Cindolo, A. Contin, M. Corradi, S. De Pasquale, I. Gialas[3], P. Giusti, G. Iacobucci, G. Laurenti, G. Levi, A. Margotti, T. Massam, R. Nania, F. Palmonari, A. Pesci, A. Polini, F. Ricci, G. Sartorelli, Y. Zamora Garcia[4], A. Zichichi
University and INFN Bologna, Bologna, Italy [f]

C. Amelung, A. Bornheim, I. Brock, K. Coböken, J. Crittenden, R. Deffner, M. Eckert, M. Grothe, H. Hartmann, K. Heinloth, L. Heinz, E. Hilger, H.-P. Jakob, U.F. Katz, R. Kerger, E. Paul, M. Pfeiffer, Ch. Rembser[5], J. Stamm, R. Wedemeyer[6], H. Wieber
Physikalisches Institut der Universität Bonn, Bonn, Germany [c]

D.S. Bailey, S. Campbell-Robson, W.N. Cottingham, B. Foster, R. Hall-Wilton, M.E. Hayes, G.P. Heath, H.F. Heath, D. Piccioni, D.G. Roff, R.J. Tapper
H.H. Wills Physics Laboratory, University of Bristol, Bristol, U.K. [o]

M. Arneodo[7], R. Ayad, M. Capua, A. Garfagnini, L. Iannotti, M. Schioppa, G. Susinno
Calabria University, Physics Dept.and INFN, Cosenza, Italy [f]

J.Y. Kim, J.H. Lee, I.T. Lim, M.Y. Pac[8]
Chonnam National University, Kwangju, Korea [h]

A. Caldwell[9], N. Cartiglia, Z. Jing, W. Liu, B. Mellado, J.A. Parsons, S. Ritz[10], S. Sampson, F. Sciulli, P.B. Straub, Q. Zhu
Columbia University, Nevis Labs., Irvington on Hudson, N.Y., USA [q]

P. Borzemski, J. Chwastowski, A. Eskreys, Z. Jakubowski, M.B. Przybycień, M. Zachara, L. Zawiejski
Inst. of Nuclear Physics, Cracow, Poland [j]

L. Adamczyk[11], B. Bednarek, M. Bukowy, K. Jeleń, D. Kisielewska, T. Kowalski, M. Przybycień, E. Rulikowska-Zarębska, L. Suszycki, J. Zając
Faculty of Physics and Nuclear Techniques, Academy of Mining and Metallurgy, Cracow, Poland [j]

Z. Duliński, A. Kotański
Jagellonian Univ., Dept. of Physics, Cracow, Poland [k]

G. Abbiendi[12], L.A.T. Bauerdick, U. Behrens, H. Beier, J.K. Bienlein, G. Cases[13], O. Deppe, K. Desler, G. Drews, U. Fricke, D.J. Gilkinson, C. Glasman, P. Göttlicher, J. Große-Knetter, T. Haas, W. Hain, D. Hasell, K.F. Johnson[14], M. Kasemann, W. Koch, U. Kötz, H. Kowalski, J. Labs, L. Lindemann, B. Löhr, M. Löwe[15], O. Mańczak, J. Milewski, T. Monteiro[16], J.S.T. Ng[17], D. Notz, K. Ohrenberg[18], I.H. Park[19], A. Pellegrino, F. Pelucchi, K. Piotrzkowski, M. Roco[20], M. Rohde, J. Roldán, J.J. Ryan, A.A. Savin, U. Schneekloth, F. Selonke, B. Surrow, E. Tassi, T. Voß[21], D. Westphal, G. Wolf, 14 U. Wollmer[22], C. Youngman, A.F. Żarnecki, W. Zeuner
Deutsches Elektronen-Synchrotron DESY, Hamburg, Germany

B.D. Burow, H.J. Grabosch, A. Meyer, S. Schlenstedt
DESY-IfH Zeuthen, Zeuthen, Germany

G. Barbagli, E. Gallo, P. Pelfer
University and INFN, Florence, Italy [f]

G. Maccarrone, L. Votano
INFN, Laboratori Nazionali di Frascati, Frascati, Italy [f]

A. Bamberger, S. Eisenhardt, P. Markun, T. Trefzger[23], S. Wölfle
Fakultät für Physik der Universität Freiburg i.Br., Freiburg i.Br., Germany [c]

J.T. Bromley, N.H. Brook, P.J. Bussey, A.T. Doyle, D.H. Saxon, L.E. Sinclair, E. Strickland, M.L. Utley[24],
R. Waugh, A.S. Wilson
Dept. of Physics and Astronomy, University of Glasgow, Glasgow, U.K. [o]

I. Bohnet, N. Gendner, U. Holm, A. Meyer-Larsen, H. Salehi, K. Wick
Hamburg University, I. Institute of Exp. Physics, Hamburg, Germany [c]

L.K. Gladilin[25], D. Horstmann, D. Kçira, R. Klanner, E. Lohrmann, G. Poelz, W. Schott[26], F. Zetsche
Hamburg University, II. Institute of Exp. Physics, Hamburg, Germany [c]

T.C. Bacon, I. Butterworth, J.E. Cole, V.L. Harris, G. Howell, B.H.Y. Hung, L. Lamberti[27], K.R. Long,
D.B. Miller, N. Pavel, A. Prinias[28], J.K. Sedgbeer, D. Sideris, A.F. Whitfield[29]
Imperial College London, High Energy Nuclear Physics Group, London, U.K. [o]

U. Mallik, S.M. Wang, J.T. Wu
University of Iowa, Physics and Astronomy Dept., Iowa City, USA [p]

P. Cloth, D. Filges
Forschungszentrum Jülich, Institut für Kernphysik, Jülich, Germany

J.I. Fleck[5], T. Ishii, M. Kuze, M. Nakao, K. Tokushuku, S. Yamada, Y. Yamazaki[30]
Institute of Particle and Nuclear Studies, KEK, Tsukuba, Japan [g]

S.H. An, S.B. Lee, S.W. Nam[31], H.S. Park, S.K. Park
Korea University, Seoul, Korea [h]

F. Barreiro, J.P. Fernández, G. García, R. Graciani, J.M. Hernández, L. Hervás[5], L. Labarga, M. Martínez,
J. del Peso, J. Puga, J. Terrón[32], J.F. de Trocóniz
Univer. Autónoma Madrid, Depto de Física Teórica, Madrid, Spain [n]

F. Corriveau, D.S. Hanna, J. Hartmann, L.W. Hung, J.N. Lim, W.N. Murray, A. Ochs, M. Riveline,
D.G. Stairs, M. St-Laurent, R. Ullmann
McGill University, Dept. of Physics, Montréal, Québec, Canada [a], [b]

T. Tsurugai
Meiji Gakuin University, Faculty of General Education, Yokohama, Japan

V. Bashkirov, B.A. Dolgoshein, A. Stifutkin
Moscow Engineering Physics Institute, Moscow, Russia [l]

G.L. Bashindzhagyan, P.F. Ermolov, Yu.A. Golubkov, L.A. Khein, N.A. Korotkova, I.A. Korzhavina,
V.A. Kuzmin, O.Yu. Lukina, A.S. Proskuryakov, L.M. Shcheglova[33], A.N. Solomin[33], S.A. Zotkin
Moscow State University, Institute of Nuclear Physics, Moscow, Russia [m]

C. Bokel, M. Botje, N. Brümmer, F. Chlebana[20], J. Engelen, P. Kooijman, A. van Sighem, H. Tiecke,
N. Tuning, W. Verkerke, J. Vossebeld, M. Vreeswijk[5], L. Wiggers, E. de Wolf
NIKHEF and University of Amsterdam, Amsterdam, Netherlands [i]

D. Acosta, B. Bylsma, L.S. Durkin, J. Gilmore, C.M. Ginsburg, C.L. Kim, T.Y. Ling, P. Nylander,
T.A. Romanowski[34]
Ohio State University, Physics Department, Columbus, Ohio, USA [p]

H.E. Blaikley, R.J. Cashmore, A.M. Cooper-Sarkar, R.C.E. Devenish, J.K. Edmonds, N. Harnew, M. Lancaster[35], J.D. McFall, C. Nath, V.A. Noyes[28], A. Quadt, O.C. Ruske, J.R. Tickner, H. Uijterwaal, R. Walczak, D.S. Waters
Department of Physics, University of Oxford, Oxford, U.K. [o]

A. Bertolin, R. Brugnera, R. Carlin, F. Dal Corso, U. Dosselli, S. Limentani, M. Morandin, M. Posocco, L. Stanco, R. Stroili, C. Voci
Dipartimento di Fisica dell' Università and INFN, Padova, Italy [f]

J. Bulmahn, R.G. Feild[36], B.Y. Oh, J.R. Okrasiński, J.J. Whitmore
Pennsylvania State University, Dept. of Physics, University Park, PA, USA [q]

Y. Iga
Polytechnic University, Sagamihara, Japan [g]

G. D'Agostini, G. Marini, A. Nigro, M. Raso
Dipartimento di Fisica, Univ. 'La Sapienza' and INFN, Rome, Italy [f]

J.C. Hart, N.A. McCubbin, T.P. Shah
Rutherford Appleton Laboratory, Chilton, Didcot, Oxon, U.K. [o]

D. Epperson, C. Heusch, J.T. Rahn, H.F.-W. Sadrozinski, A. Seiden, D.C. Williams
University of California, Santa Cruz, CA, USA [p]

O. Schwarzer, A.H. Walenta
Fachbereich Physik der Universität-Gesamthochschule Siegen, Germany [c]

H. Abramowicz[37], G. Briskin, S. Dagan[37], S. Kananov[37], A. Levy[37]
Raymond and Beverly Sackler Faculty of Exact Sciences, School of Physics, Tel-Aviv University, Tel-Aviv, Israel [e]

T. Abe, T. Fusayasu, M. Inuzuka, K. Nagano, I. Suzuki, K. Umemori, T. Yamashita
Department of Physics, University of Tokyo, Tokyo, Japan [g]

R. Hamatsu, T. Hirose, K. Homma, S. Kitamura[38], T. Matsushita, K. Yamauchi
Tokyo Metropolitan University, Dept. of Physics, Tokyo, Japan [g]

R. Cirio, M. Costa, M.I. Ferrero, S. Maselli, V. Monaco, C. Peroni, M.C. Petrucci, R. Sacchi, A. Solano, A. Staiano
Università di Torino, Dipartimento di Fisica Sperimentale and INFN, Torino, Italy [f]

M. Dardo
II Faculty of Sciences, Torino University and INFN - Alessandria, Italy [f]

D.C. Bailey, M. Brkic, C.-P. Fagerstroem, G.F. Hartner, K.K. Joo, G.M. Levman, J.F. Martin, R.S. Orr, S. Polenz, C.R. Sampson, D. Simmons, R.J. Teuscher[5]
University of Toronto, Dept. of Physics, Toronto, Ont., Canada [a]

J.M. Butterworth, C.D. Catterall, T.W. Jones, P.B. Kaziewicz, J.B. Lane, R.L. Saunders, J. Shulman, M.R. Sutton
University College London, Physics and Astronomy Dept., London, U.K. [o]

B. Lu, L.W. Mo
Virginia Polytechnic Inst. and State University, Physics Dept., Blacksburg, VA, USA [q]

J. Ciborowski, G. Grzelak[39], M. Kasprzak, K. Muchorowski[40], R.J. Nowak, J.M. Pawlak, R. Pawlak, T. Tymieniecka, A.K. Wróblewski, J.A. Zakrzewski
Warsaw University, Institute of Experimental Physics, Warsaw, Poland [j]

M. Adamus
Institute for Nuclear Studies, Warsaw, Poland [j]

C. Coldewey, Y. Eisenberg[37], D. Hochman, U. Karshon[37], D. Revel[37]
Weizmann Institute, Department of Particle Physics, Rehovot, Israel [d]

W.F. Badgett, D. Chapin, R. Cross, S. Dasu, C. Foudas, R.J. Loveless, S. Mattingly, D.D. Reeder,
W.H. Smith, A. Vaiciulis, M. Wodarczyk
University of Wisconsin, Dept. of Physics, Madison, WI, USA [p]

S. Bhadra, W.R. Frisken, M. Khakzad, W.B. Schmidke
York University, Dept. of Physics, North York, Ont., Canada [a]

1 Introduction

A number of studies have been made at HERA on the properties of hard processes in quasi-real photo-production [1–8]. In lowest order QCD, two major types of $2 \to 2$ process can be defined, depending on how the photon interacts with a parton in the proton: direct, in which the photon interacts as a pointlike particle in the hard subprocess, and resolved, in which the photon provides a quark or gluon which then interacts. The outgoing products of these subprocesses are most commonly quarks or gluons, which at high transverse energy (E_T) can give rise to two observed jets (dijet events). However, final states containing a high-E_T jet together with a high-E_T photon are also possible (fig. 1). Such photons are known as "prompt" photons to distinguish them from those produced via particle decays. In the kinematic region accessible with ZEUS, the direct channel in prompt photon processes is expected to be dominated by the direct Compton process $\gamma q \to \gamma q$, i.e. by the elastic scattering of a photon by a quark in the proton. The main predicted contributions to the resolved processes are $qg \to q\gamma$ and $q\bar{q} \to g\gamma$ [9].

A further source of prompt photons is dijet events in which an outgoing quark radiates a high-E_T photon. In measuring prompt photon processes, these radiative contributions are largely suppressed by restricting the measurement to prompt photons that are isolated from other particles in the event. Such a condition is also needed in order to reduce experimental backgrounds from neutral mesons in jets.

In hadronic collisions, both with fixed targets [10] and colliders [11, 12], prompt photon processes provide a means to study the gluon content of the proton [13, 14]. Fixed target studies [15] have also provided a first confirmation of prompt photon processes in photoproduction, at a level consistent with QCD expectations. At HERA, the highly asymmetric beam energies, together with the present detector coverage, restrict the sensitivity of the resolved processes to the quark content of the photon [16, 17, 18] and the quark and gluon contents of the proton. A particular advantage of prompt photon processes is that the observed final-state photon emerges from the hard process directly, without the intermediate hadronisation by which a final state quark or gluon forms an observable jet. The cross section of the direct Compton process depends only on the quark charge, together with the quark density in the proton. The above considerations, together with the availability of next-to-leading order (NLO) calculations [17, 19, 20], make prompt photon processes an attractive and relatively clean means for studying QCD, despite the low cross sections.

From data taken in e^+p running in 1995 with the ZEUS detector at HERA, we have identified a class of events showing the characteristics of hard prompt photon processes in quasi-real γp collisions. A strong signal is obtained, and the presence of the direct process is clearly seen. This is the first observation of prompt photons at γp centre of mass energies an order of magnitude higher than those previously employed. The data are compared with leading order Monte Carlo predictions. The cross section for the photoproduction of a prompt photon and a jet within a defined set of kinematic cuts is evaluated and compared with an NLO QCD calculation.

2 Apparatus and trigger

The data used in the present analysis were collected with the ZEUS detector at HERA. During 1995, HERA collided positrons of energy $E_e = 27.5$ GeV with protons of energy $E_p = 820$ GeV, in 173 circulating bunches. Additional unpaired positron (15) and proton (7) bunches enabled monitoring of beam related backgrounds. The data sample used in this analysis corresponds to an integrated luminosity of 6.36 pb^{-1}. The luminosity was measured by means of the positron-proton bremsstrahlung process $ep \to e\gamma p$, using a lead-scintillator calorimeter at $Z = -107$ m[1] which detects photons radiated at angles of less than 0.5 mrad to the positron beam direction.

The ZEUS apparatus is described elsewhere [1]. Of particular importance in the present work are the uranium calorimeter and the central tracking detector (CTD). The calorimeter [21] has an angular coverage

---

[1] The ZEUS coordinate system has positive-Z in the proton beam direction, with a horizontal X-axis pointing towards the centre of HERA. The nominal interaction point is at $X = Y = Z = 0$. Pseudorapidity η is defined as $-\ln\tan(\theta/2)$, where θ is the polar angle relative to the Z direction. In the present analysis η is always defined in the laboratory frame, and the Z position of the event vertex is taken into account.

of 99.7% of 4π and is divided into three parts (FCAL, BCAL, RCAL), covering the forward (proton direction), central and rear polar angle ranges 2.6°–36.7°, 36.7°–129.1°, and 129.1°–176.2°, respectively. Each part consists of towers longitudinally subdivided into electromagnetic (EMC) and hadronic (HAC) cells. In test beam measurements, energy resolutions of $\sigma_E/E = 0.18/\sqrt{E}$ for electrons and $\sigma_E/E = 0.35/\sqrt{E}$ for hadrons have been obtained (with E in GeV). The calorimeter cells also provide time measurements which are used for beam gas background rejection. The electromagnetic sections of the FCAL and RCAL comprise non-projective cells of transverse dimensions 20×5 and 20×10 cm^2 respectively. The electromagnetic section of the BCAL (BEMC) consists of cells of approximate dimensions 5×20 cm^2, with the finer dimension in the Z direction. These cells have a projective geometry so as to present a uniform granularity to particles emerging from the interaction point. In this analysis, we employ the BEMC to identify photons with $E_T \geq 5$ GeV. At these energies, the separation of the photons from a π^0 decay is of similar magnitude to the BEMC cell width, whereas the width of a single electromagnetic shower in the BEMC is characterised by a Molière radius of 2 cm. The profile of electromagnetic signals (i.e. clusters of cells) in the BEMC thus gives a partial discrimination between those originating from single photons or electrons/positrons, and those originating from the decay of neutral mesons.

The CTD is a cylindrical drift chamber [22] situated inside a superconducting magnet coil which produces a 1.43 T field. It consists of 72 cylindrical layers covering the polar angle region $15° < \theta < 164°$. Using the tracking information from the CTD, the vertex of an event can be reconstructed with a resolution of 0.4 cm in Z and 0.1 cm in X, Y. In the present analysis the CTD tracks are used to locate the event vertex, to discriminate between high-E_T photons and electrons/positrons, and in the photon isolation criterion to be described below.

For jet identification, a cone algorithm in accordance with the Snowmass Convention [3, 23] was applied to the calorimeter cells, each energy deposit in a calorimeter cell being treated as if corresponding to a massless particle. A cone radius $R = \sqrt{(\delta\phi)^2 + (\delta\eta)^2}$ of 1.0 was used, where $\delta\phi, \delta\eta$ denote the distances of the cells from the centre of the jet in azimuth and pseudorapidity. The same algorithm was used online for triggering and also in the offline analysis.

The ZEUS detector uses a three-level trigger system. The first-level trigger used in the present analysis selected events on the basis of a coincidence of a regional or transverse energy sum in the calorimeter and at least one track in the CTD pointing towards the interaction point. At the second level, at least 8 GeV of transverse energy was demanded, excluding the eight calorimeter towers surrounding the forward beam pipe. Cuts on calorimeter energies and timing were imposed to suppress events arising from proton-gas collisions in the beam pipe. At the third level, jets were identified with $\eta^{jet} < 2.5$, and at least two jets with $E_T^{jet} > 4$ GeV were demanded. These included high-E_T photons. Cosmic ray events were rejected by means of information from the tracking chambers and calorimeter. An event vertex with $|Z| < 60$ cm was required. The trigger efficiency is estimated at 97% for the events of the present analysis.

3   Event selection

In the offline analysis, candidate prompt photon signals in the BCAL were selected by means of an algorithm which identified clusters of firing cells whose energy was predominantly in the BEMC. The algorithm did not use tracking information, and was based on one developed for the identification of deep inelastic scattered (DIS) electrons [24]. Events were retained for subsequent analysis if a photon candidate with transverse energy $E_T^\gamma \geq 4.5$ GeV was found in the BCAL. The BCAL requirement restricts photon candidates to the approximate pseudorapidity range $-0.75 < \eta^\gamma < 1.0$.

A photon candidate was rejected if a track pointed within 0.3 radian of it; high-E_T positrons and electrons were thus removed, including the majority of those that underwent hard radiation in the material between the interaction point and the BCAL. If more than one acceptable candidate was found, the one with highest E_T was taken. Approximately 2.7k events remained at this stage.

Events having an identified DIS positron in addition to the BCAL photon candidate were removed, restricting the acceptance of the present analysis to incident photons of virtuality $Q^2 \lesssim 1$ GeV^2. For the remaining events, $y_{JB} = \sum(E - p_Z)/2E_e$ was calculated, where the sum is over all calorimeter cells,

treating each signal as equivalent to a massless particle; i.e. E is the energy deposited in the cell, and p_Z is the value of $E\cos\theta$. The quantity y_{JB} is a measure of $y^{true} = E_{\gamma,\,in}/E_e$, where $E_{\gamma,\,in}$ is the energy of the incident photon. In the case that an unidentified DIS positron is present, a value of approximately unity is obtained. A requirement of $0.15 < y_{JB} < 0.7$ was imposed, the lower cut removing some residual proton-gas backgrounds and the upper cut removing remaining DIS events. This thereby eliminates any remaining prompt photon candidates which were in actual fact misidentified DIS positrons. Wide-angle QED Compton scatters $(e(p) \rightarrow e\gamma(p))$ were also excluded by this cut.

A jet with transverse energy $E_T^{jet} > 4.5$ GeV and pseudorapidity $-1.5 \leq \eta^{jet} \leq 1.8$ was also demanded. If more than one such jet was found, that with the highest transverse energy was used in the analysis.

An isolation cone was now imposed around the photon candidate: within a cone of unit radius in $(\eta,\,\phi)$, the total E_T from other particles was required not to exceed $0.1E_T^{\gamma}$. This was calculated by summing the E_T in each calorimeter cell within the isolation cone, treating each cell energy as equivalent to that of a massless particle. Additional contributions were included from charged tracks which started within the isolation cone but curved out of it; the small number of tracks which curved into the isolation cone were ignored. This isolation condition greatly reduces the dijet background, by removing the large majority ($\approx$80%) of events where the photon candidate is associated with a jet, and is therefore either hadronic in origin or else a photon radiated within a jet. In particular, as discussed by previous authors [17], it removes most dijet events in which a photon is radiated from a final state quark. The losses of direct and resolved prompt photon events due to the isolation condition were found from Monte Carlo studies to be $\approx$5% and $\approx$17% respectively. Overall, the isolation condition removed 70% of the candidates remaining at this stage, leaving 568 events.

Some tighter kinematic conditions were finally applied. The photon candidate was required to have $5 \leq E_T^{\gamma} < 10$ GeV, the upper limit being imposed due to the increasing difficulties in distinguishing photons from π^0 in the BEMC above this energy. As will be seen below, the photons and jets were found to be azimuthally back-to-back in the detector, and no evidence for a photon signal was found in the candidates where the azimuthal separation $\Delta\phi$ between the photon candidate and the jet was less than 140°. $\Delta\phi$ was therefore required to be above 140° for the final event sample. The number of events remaining at this stage was 256.

4   Analysis method

4.1   Monte Carlo simulations

Three types of Monte Carlo samples were employed in this analysis to simulate: (1) the prompt photon processes, (2) single particles $(\gamma,\ \pi^0,\ \eta)$, and (3) dijet processes that could mimic a prompt photon final state. All generated events were passed through a full simulation of the ZEUS detector.

The PYTHIA-5.7 [25] Monte Carlo generator was used to simulate the direct and resolved prompt photon processes and dijet processes. The MRSA proton structure function and GRV(LO) photon structure function were employed. The minimum p_T of the hard scatter was set to 2.5 GeV and the maximum Q^2 set to 4 GeV^2. In running PYTHIA, initial and final state QCD and QED radiation were turned on. Multiple interactions were not included in the resolved event sample since they are not expected to have a significant effect in the present analysis.

Three additional Monte Carlo data sets were generated, comprising large samples of single γ, π^0 and η respectively. The single particles were generated over the acceptance of the BCAL with a flat transverse energy distribution between 3 and 20 GeV; E_T-dependent exponential weighting functions were subsequently applied to reproduce the observed E_T distributions. These samples are important for the understanding and the separation of signal and background using shower shapes in the calorimeter.

To produce a Monte Carlo sample for background studies, direct and resolved dijet events were generated. Event samples of this kind also enabled the radiative contribution to the prompt photon signal to be evaluated. Measurements from ALEPH [26] have shown that the PYTHIA generator gives a qualitative description of this type of process in e^+e^- annihilation, but that the magnitude may be underestimated.

4.2   Identification of photon signal

Electromagnetic signals in the calorimeter that do not arise from charged particles arise predominantly from photons and from π^0 and η mesons. The minimum distance at the BCAL between the photons from a π^0 with $E_T = 5$ (10) GeV is 7 (3.5) cm, which is comparable to the Z width of the BEMC cells and smaller than the azimuthal cell width. Thus it is not normally possible to resolve the two photons from a π^0 and hence reconstruct its decay. The $\eta \to 2\gamma$ decay angle, although broader by a factor of three than the π^0, is still unresolvable in most cases, while the $\eta \to 3\pi^0$ mode gives up to six photon signals which may be varyingly merged together. It is therefore not possible to distinguish single photons from the π^0 and η backgrounds on an event-by-event basis.

A typical high-E_T photon candidate in the BEMC consists of a cluster of 4-5 cells selected by the electron finder. Two shape-dependent quantities were studied in order to distinguish photon, π^0 and η signals. These were (i) the mean width $<\delta Z>$ of the BEMC cluster in Z and (ii) the fraction f_{max} of the photon candidate energy found in the most energetic cell in the cluster. $<\delta Z>$ is defined as the mean absolute deviation in Z of the cells in the cluster, energy weighted, measured from the energy weighted mean Z value of the cells in the cluster. It is expressed in units of the BEMC cell width in the Z direction.

From the Monte Carlo samples of single γ, π^0 and η in the BCAL, it was established that the photon and π^0 signals both had small probabilities of having $<\delta Z> \geq 0.65$. A cut was therefore imposed at this value, separating candidates with $<\delta Z> \geq 0.65$, taken to be mainly η mesons, from those in the lower $<\delta Z>$ range, which comprised mainly photons and π^0 mesons with a small admixture of η. The f_{max} distribution for the sample of events with $<\delta Z> < 0.65$ is shown in fig. 2. A fit to a mixture of γ, π^0 and η was performed on this f_{max} distribution, together with the numbers of events with $<\delta Z> \geq 0.65$, which determined the η contribution. From the fit it is evident that the η and π^0 f_{max} distributions are similar in shape, whereas the photon f_{max} distribution has a sharp peak above a value 0.75. The fit to the experimental f_{max} distribution is good, and above 0.75 the data are dominated by a substantial photon component.

As a check on the procedure, the f_{max} distribution of deep inelastic scattered positrons in the BCAL was compared with a corresponding Monte Carlo sample. A small discrepancy in the mean positions of the two peaks was found; as a consequence all the plotted Monte Carlo f_{max} values have been scaled by a factor 1.025±0.005. This gives rise to a systematic uncertainty in the final results of ±4%.

We perform a background subtraction on the assumption that the data may be expressed as a sum of photon signal plus neutral meson background as indicated in fig. 2. An important conclusion from fig. 2 is that the shape of the f_{max} distribution is similar for the η and π^0 contributions. It follows that the background subtraction is insensitive to uncertainties in the ratio of π^0 to η in the fit.

4.3   Signal/background separation

Guided by fig. 2, we divide the data into two subsamples, consisting of events whose photon candidate has $f_{max} \geq 0.75$ and $f_{max} < 0.75$ respectively. Such subsamples are respectively enriched and impoverished in events containing a genuine high-E_T photon, and will be referred to as "good" and "poor" subsamples. In any given bin of a physical quantity of interest, using the same definition, the events can be likewise divided into good and poor subsamples. Let these consist of n_{good} and n_{poor} events respectively. The values of n_{good} and n_{poor} in a bin may be written:

$$
\begin{aligned}
n_{good} &= \alpha\, n_{sig} + \beta\, n_{bgd} \\
n_{poor} &= (1-\alpha)n_{sig} + (1-\beta)n_{bgd}
\end{aligned}
\tag{1}
$$

where n_{sig}, n_{bgd} are numbers of signal (i.e. photon) and background (i.e. π^0 or η) events in the bin. The coefficients α (β) are the probabilities that a signal (background) event will end up in the good subsample. They are evaluated from the known shapes of the Monte Carlo f_{max} distributions of the photons and of the fitted $\pi^0 + \eta$ background, as shown in fig. 2. For given observed values of n_{good} and n_{poor} it is now straightforward to solve (1) for the values of n_{sig} and n_{bgd}, and to evaluate their errors.

5 Results

Fig. 3(a) shows that the background-subtracted distribution of the azimuthal angle difference ($\Delta\phi$) between the photon and the accompanying jet is well peaked at 180° as expected. Also shown are the corresponding Monte Carlo expectations for contributions from: (i) dijet events in which an outgoing quark radiates an isolated high-E_T photon; (ii) the resolved prompt photon processes; (iii) direct prompt photon production. Here and in fig. 4, the Monte Carlo distributions are normalised to the same integrated luminosity as the data. For clarity, the plotted histograms show (i), (i)+(ii) and (i)+(ii)+(iii). The error bars on the data points are statistical only. Reasonable agreement between the data and the sum of the Monte Carlo distributions is seen. Fig. 3(b) shows the difference in transverse energy between the photon and the jet for the virtually background-free class of events with $x_\gamma^{meas} > 0.9$ (see below). The E_T of the photon and jet are on average well balanced, and the shape of the Monte Carlo satisfactorily reproduces that of the data.

The fraction x_γ of the incoming photon momentum that contributes to the production of the high-E_T photon and jet is studied. For the case of a direct process (as defined at leading order), $x_\gamma = 1$. Here we estimate the "observable" quantity $x_\gamma^{\mathrm{OBS}} = (E_{T\,1}e^{-\eta_1} + E_{T\,2}e^{-\eta_2})/2E_e y^{true}$ [3] as

$$x_\gamma^{meas} = \sum_{\gamma,\,jet} \left(E - p_Z\right)/2E_e\, y_{JB}.$$

The sums are over the photon candidate and the calorimeter cells in the jet, each signal being treated as equivalent to that of a massless particle of energy E and longitudinal momentum component p_Z. The distribution of the resulting signal is shown in fig. 4(a). A narrow peak is seen in the signal near $x_\gamma^{meas} = 1$, which we identify with the direct Compton process. The bin widths at the peak are chosen to be comparable to the measurement resolution on x_γ^{meas} in this region (0.035), and are governed by the statistics elsewhere. The Monte Carlo distribution is similar in shape and magnitude. QCD radiation, hadronisation outside the jet cone and detector effects lower the peak position slightly from its expected value of unity. There is, in addition, a tail of entries extending over lower x_γ^{meas} values. It is not possible to draw conclusions concerning the presence of a resolved photon component, except to remark that the observed numbers of events at low x_γ^{meas} are consistent with the level expected from the Monte Carlo. The predicted radiative contribution is not negligible compared to the resolved contribution. For $x_\gamma^{meas} > 0.8$, the number of events in the signal is 57.6; the size of the signal is insensitive to small variations in the isolation conditions. The Monte Carlo calculations indicate that approximately 75% of the events in this region are direct Compton, 12% are resolved and 13% are radiative. It should be noted that the effects of higher order QCD processes are not included in the present Monte Carlo simulation.

The background distribution is consistent with zero for $x_\gamma^{meas} > 0.9$. Below this value it averages at two counts per 0.025 interval of x_γ^{meas}. As a test of the procedure, an identical analysis was performed using the photon candidates obtained in the Monte Carlo dijet samples, excluding the events where an outgoing quark radiates a photon. These candidates were due to a physically realistic mixture of simulated neutral mesons. Here, results were obtained consistent with zero prompt photon signal, accompanied by the expected finite background.

The simulations make use of parton densities in the proton in a region of x_p (the fraction of the proton's momentum entering the hard process) where these are experimentally well known. A value of x_p is calculated analogously to x_γ^{meas} as $x_p^{meas} = \sum_{\gamma,\,jet}(E + p_Z)/2E_p$. Fig. 4(b) shows the distribution of x_p^{meas} compared to the predictions from PYTHIA. Again, reasonable agreement between experiment and Monte Carlo is seen.

A systematic uncertainty exists in the comparison of the data with the Monte Carlo, due to an estimated 3% uncertainty on the calorimeter calibration. Rescaling the calorimeter cell energies in the direct prompt photon MC by ±3% changes the number of events accepted by ±8%. The E_T weighting of the generated single particles was also varied by amounts corresponding to the experimental uncertainty on the E_T distributions of these particles. In each case, the results were affected by approximately 1%. The f_{max} distributions exhibited by the single particle MC samples, and by the data, varied little with the pseudorapidity of the particles. To test for sensitivity to this, an analysis was performed using Monte Carlo photons generated only in the range $|\eta^\gamma| > 0.35$, and applying the f_{max} distribution of this sample

to the data in place of the standard distribution. This changed the results by $\approx 3\%$. It is possible that the $\eta : \pi^0$ ratio in the background might vary from bin to bin in a given physical quantity. To evaluate the possible effects of this, we performed a fit in which the $\eta : \pi^0$ ratio in the background was halved from its normal value. This altered the final results by about 1%.

A cross section for the prompt photon process is evaluated as follows. The number n_0 of observed events in a given x_γ^{meas} range is determined, subject to the experimental selection conditions stated above. From Monte Carlo event samples, we evaluate the number of fully reconstructed events subject to the same conditions as the data (n_1), and the number of events satisfying a set of defined conditions at the final-state hadron level (n_2). These latter conditions are chosen, taking experimental effects into account, to be approximately equivalent to the selection conditions on the data. The ratio n_2/n_1 then represents a correction factor to be applied to n_0, to give an experimental cross section for the process defined by the conditions used to evaluate n_2.

We quote a cross section for the process

$$ep \rightarrow e + \gamma_{prompt} + jet + X$$

with $x_\gamma^{\text{OBS}} \geq 0.8$. Here, γ_{prompt} denotes a final state isolated prompt photon with $5 \leq E_T^\gamma < 10$ GeV and $-0.7 \leq \eta^\gamma < 0.8$; jet denotes a "hadron jet" with $E_T^{jet} \geq 5$ GeV and $-1.5 \leq \eta^{jet} \leq 1.8$. X includes the proton remnant, a possible photon remnant and any other final state products. A "hadron jet" is a jet constructed out of the primary final state particles (charged or uncharged) in a given Monte Carlo generated event. The energy and direction of each primary final state particle are used in the jet finder in the same way as the calorimeter cells are used in the experimental jet finding. Limits of $0.16 < y^{true} < 0.8$ and $Q^2 < 1 \, \text{GeV}^2$ were applied in the hadron level event definition, and an equivalent isolation cone definition was applied as in the data, i.e. the total E_T from other particles inside a cone of unit radius around the generated prompt photon was permitted to be at most 0.1 of that of the photon. The systematic errors are dominated by the 8% contribution due to the uncertainty in the calorimeter calibration. The correction factor (n_2/n_1) is 1.69±0.09, where the error comes from Monte Carlo statistics and the uncertainty in the size of the radiative contribution. A contribution of 5% is included to allow for differences between the shapes of the data and Monte Carlo distributions. As a systematic check on the Monte Carlo simulation of the noise in the calorimeter cells due to uranium radioactivity, the minimum energy deposit in a cell above which the cell enters the analysis was varied. The change in the cross section was 2%.

With the above definitions, a cross section of 15.3±3.8±1.8 pb is obtained, where the errors are statistical and systematic respectively. This result can be compared with NLO calculations at the parton level of Gordon [27] (using an LO radiative contribution), in which the integrated cross section for the process $ep \rightarrow e + \gamma_{prompt} + jet + X$ is evaluated under the same kinematic conditions as used above. Using the GS and GRV NLO [28] photon parton densities, integrated cross sections of 14.05 (13.17) pb and 17.93 (16.58) pb respectively are obtained, where the first value is calculated at a QCD scale $\mu = 0.25 \, (E_T^\gamma)^2$ and the second, parenthesized value at $\mu = (E_T^\gamma)^2$. These values cover the range of theoretical uncertainty of each calculation. The experiment and theory are in good agreement. The ratio of the resolved to the direct contribution in the calculated cross section is scale dependent, and takes values in the range 0.23–0.34 for the GS parton densities.

6   Conclusions

We have observed for the first time isolated high-E_T photons, accompanied by balancing jets, in photoproduction at HERA. The x_γ^{meas} distribution of the events is in good general agreement with LO QCD expectations as calculated using PYTHIA. In particular, a pronounced peak at high x_γ^{meas} is observed, indicating the presence of a direct process.

We have measured the cross section for prompt photon production in ep collisions satisfying the conditions of having (i) an isolated final-state photon with $5 \leq E_T^\gamma < 10$ GeV, accompanied by a jet with $E_T^{jet} \geq 5$ GeV, (ii) the photon and jet lying within the respective laboratory pseudorapidity ranges (−0.7, 0.8) and

$(-1.5, 1.8)$, (iii) $x_\gamma^{\rm OBS} \geq 0.8$, (iv) $0.16 < y^{true} < 0.8$, (v) $Q^2 < 1\,{\rm GeV}^2$. The value obtained is $15.3\pm3.8\pm1.8$ pb, in good agreement with a recent NLO calculation of the process.

Acknowledgements.

References

[1] ZEUS Collaboration, M. Derrick et al., Phys. Lett. **B297** (1992) 404.

[2] ZEUS Collaboration, M. Derrick et al., Phys. Lett. **B322** (1994) 287.

[3] ZEUS Collaboration, M. Derrick et al., Phys. Lett. **B348** (1995) 665.

[4] ZEUS Collaboration, M. Derrick et al., Phys. Lett. **B384** (1996) 401.

[5] H1 Collaboration, T. Ahmed et al., Phys. Lett. **B297** (1992) 205.

[6] H1 Collaboration, T. Abt et al., Phys. Lett. **B314** (1993) 436.

[7] H1 Collaboration, T. Ahmed et al., Nucl. Phys. **B445** (1995) 195.

[8] H1 Collaboration, S. Aid et al., Phys. Lett. **B392** (1997) 234.

[9] A. C. Bawa and W. J. Stirling, J. Phys. **G14** (1988) 1353;
A. C. Bawa, M. Krawczyk and W. J. Stirling, Z. Phys. **C50** (1991) 293;
A. C. Bawa and M. Krawczyk, Proc. Workshop *Physics at HERA,* eds. W. Buchmüller and G. Ingelman, DESY (1992) 579.

[10] E. Anassontzis et al., Z. Phys. **C13** (1982) 277;
WA70 Collaboration, M. Bonesini et al., Z. Phys. **C38** (1988) 371;
E706 Collaboration, G. Alverson et al., Phys. Rev. **D48** (1993) 5.

[11] UA6 Collaboration, A. Bernasconi et al., Phys. Lett. **B206** (1988) 163, G. Sozzi et al., Phys. Lett. **B317** (1993) 243;
UA2 Collaboration, J. Alitti et al., Phys. Lett. **B263** (1991) 544

[12] CDF Collaboration, F. Abe et al., Phys. Rev. **D48** (1993) 2998, Phys. Rev. Lett. **73** (1994) 2662;
D0 Collaboration, S. Abachi et al., Phys. Rev. Lett. **77** (1996) 5011.

[13] H. L. Lai et al., Phys. Rev. **D51** (1995) 4763.

[14] W. Vogelsang and A. Vogt, Nucl. Phys. **B453** (1995) 334.

[15] NA14 Collaboration, P. Astbury et al., Phys. Lett. **152B** (1985) 419; E. Auge et al., Phys. Lett. **B182** (1986) 409.

[16] L. E. Gordon and J. K. Storrow, Z. Phys. **C63** (1994) 581.

[17] L. E. Gordon and W. Vogelsang, Phys. Rev. **D50** (1994) 1901, Phys. Rev. **D52** (1995) 58.

[18] P. J. Bussey, proc. *Photon 95,* Sheffield, ed. D. J. Miller et al. (World Scientific, 1996), 47.

[19] P. Aurenche et al., Z. Phys. **C56** (1992) 589.

[20] J. Huston et al., Phys. Rev. **D51** (1995) 6139.

[21] A. Andresen et al., Nucl. Instr. Meth. **A309** (1991) 101;
A. Bernstein et al., Nucl. Instr. Meth. **A338** (1993) 23;
A. Caldwell et al., Nucl. Instr. Meth. **A321** (1992) 356.

[22] N. Harnew et al., Nucl. Instr. Meth. **A279** (1989) 290;
B. Foster et al., Nucl. Phys. **B** (Proc. Suppl.) **32** (1993) 181, Nucl. Instr. Meth. **A338** (1994) 254.

[23] J. Huth et al., in proc. 1990 DPF Summer Study on High Energy Physics, Snowmass, Colorado, ed. E. L. Berger (World Scientific, Singapore, 1992) 134.

[24] ZEUS Collaboration, M. Derrick et al., Z. Phys. **C65** (1995) 379.

[25] H.-U. Bengtsson and T. Sjöstrand, Comp. Phys. Comm. **46** (1987) 43; T. Sjöstrand, CERN-TH.6488/92.

[26] ALEPH Collaboration, D. Buskulic et al., Z. Phys. **C69** (1996) 365.

[27] L. E. Gordon, proc. *Photon 97*, Egmond aan Zee, in preparation (hep-ph/9706355), and private communication.

[28] L. E. Gordon and J. K. Storrow, Nucl. Phys. **B489** (1997) 405;
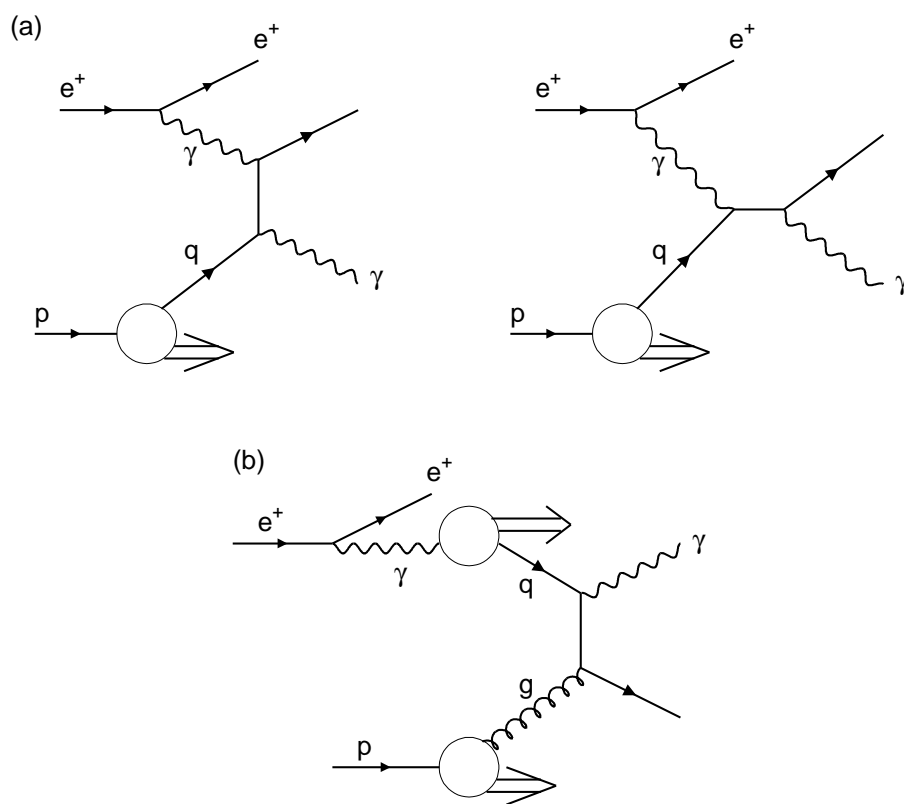M. Glück, E. Reya and A. Vogt, Phys. Rev. **D46** (1992) 1973.

Figure 1: (a) Direct LO diagrams in hard photoproduction producing an outgoing prompt photon. (b) Example of resolved process. Corresponding dijet diagrams may be obtained by replacing the final-state photon by a gluon.
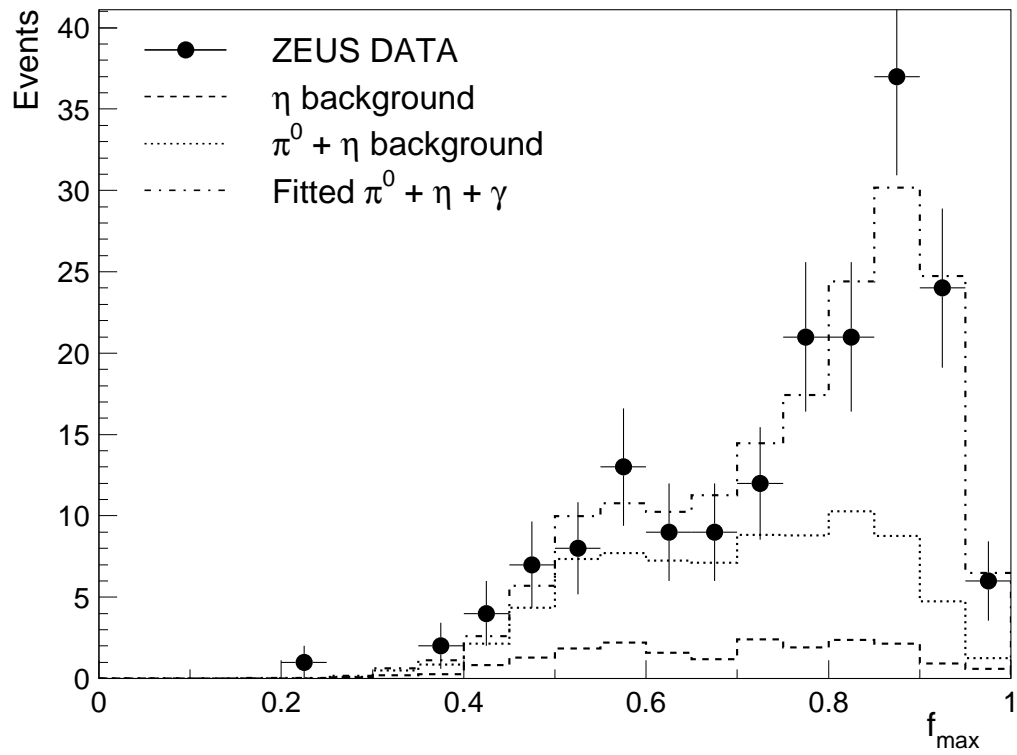
Figure 2: Distribution of f_{max} for prompt photon candidates in selected events, including a requirement that $<\delta Z> < 0.65$ cell widths. Also plotted are fitted Monte Carlo curves for photons, π^0 and η mesons with similar selection cuts as for the observed photon candidates (see text).
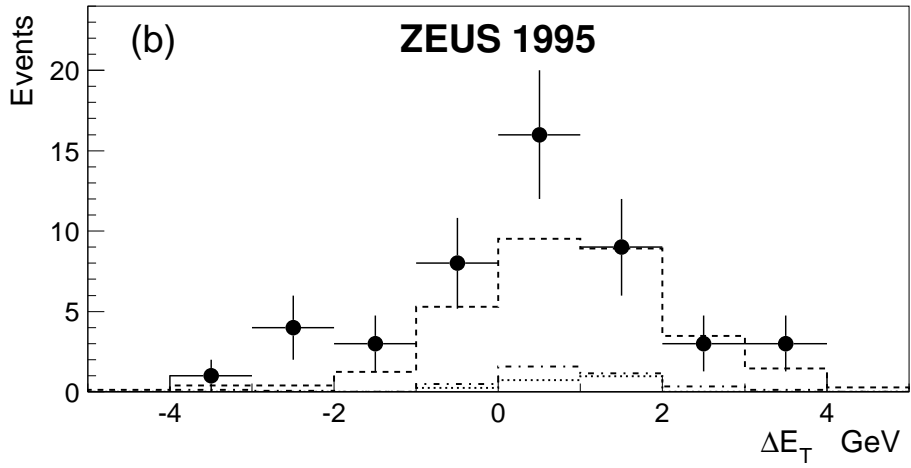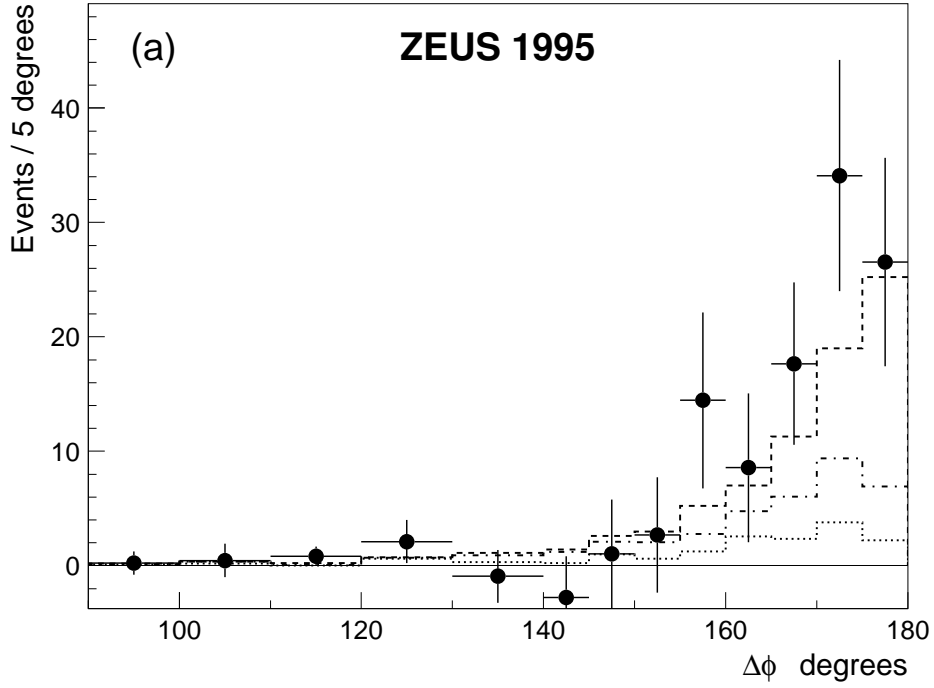
Figure 3: (a) Background subtracted distribution in $\Delta\phi$ for photon-jet pairs, before application of cut on $\Delta\phi$. (b) Distribution in $\Delta E_T = (E_T^\gamma - E_T^{jet})$ for selected events ($x_\gamma^{meas} > 0.9$, c.f. fig. 4). Points = data; dotted histogram = MC radiative contribution; dash-dotted = radiative + resolved; dashed = radiative + resolved + direct.
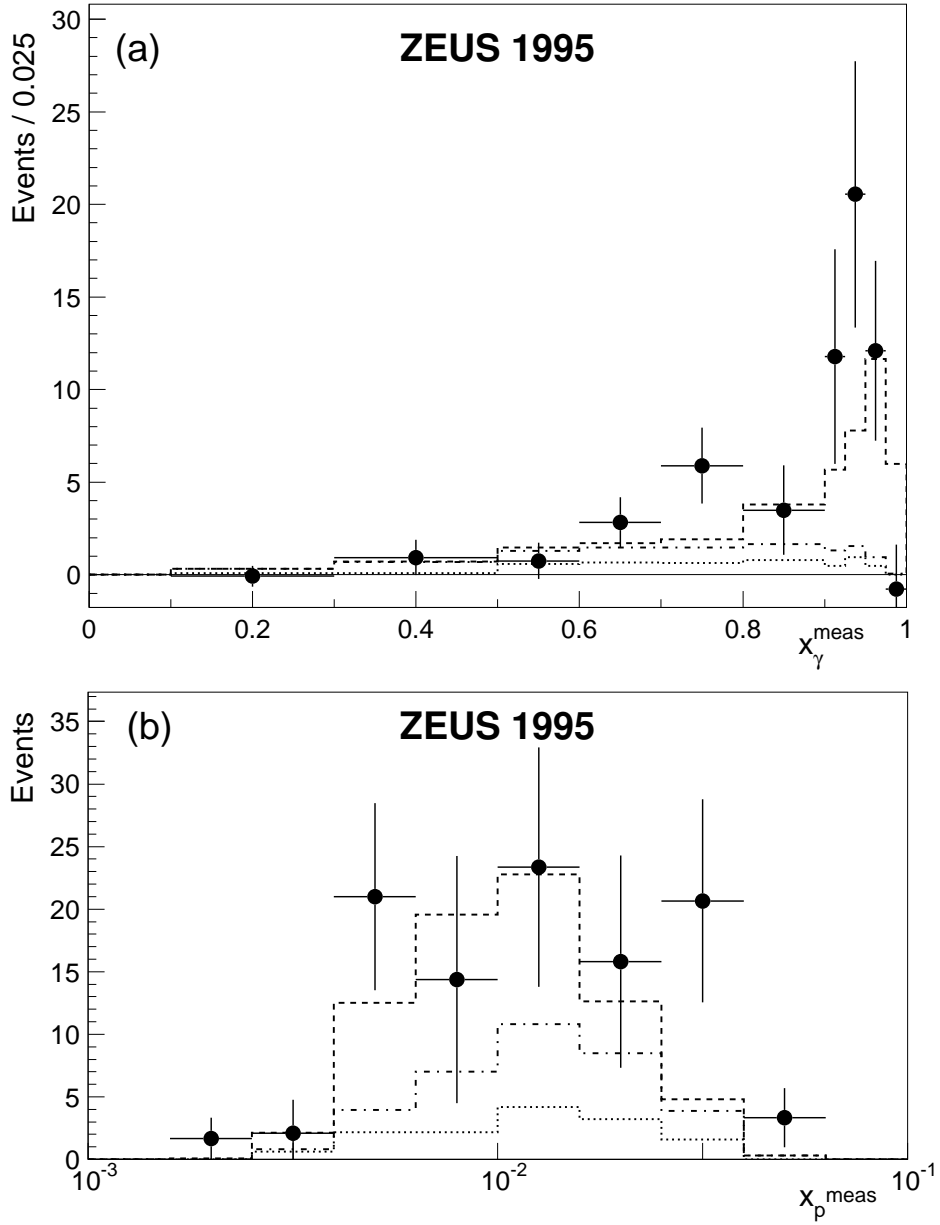
Figure 4: (a) Distribution in x_γ^{meas} of prompt photon events after background subtraction. Points = data; dotted histogram = MC radiative contribution; dash-dotted = radiative + resolved; dashed = radiative + resolved + direct. Plotted values represent numbers of events per 0.025 interval of x_γ^{meas}; i.e. total number of events in bin = plotted value × bin width / 0.025. Errors are statistical only and no corrections have been applied to the data. (b) Distribution in x_p^{meas}, data and histograms as (a); the plotted points are events per bin.